Turbulence/Shock Wave Interaction in Simulation of Underexpanded Supersonic Jets

B. Emami[1], M. Bussmann[1] and H. N. Tran[2]

[1]*Department of Mechanical and Industrial Engineering, University of Toronto Toronto, ON, M5S 3G8, Canada*

[2]*Department of Chemical Engineering and Applied Chemistry, University of Toronto Toronto, ON, M5S 3E5, Canada*

Email: *bemami@mie.utoronto.ca*

Abstract

We use an explicit cell-centered finite volume solver, coupled to a $k - \varepsilon$ turbulence model, to simulate an underexpanded supersonic air jet exhausting into still air, and compare the results to available experimental data. It is shown that the $k - \varepsilon$ turbulence model corrected for structural compressibility fails to satisfactorily predict the behavior of underexpanded jets, as the correction does not properly model the turbulence/shock wave interaction. Two approaches are then examined to account for that interaction: imposition of the realizability condition (Durbin, International Journal of Heat and Fluid Flow 17, 89-90, 1996; Thivet et al., 23rd Symposium on Shock Waves, Texas, 2001), and consideration of shock unsteadiness effects (Sinha et al., Physics of Fluids 15, 2290-2297, 2003; Sinha et al., AIAA Journal 43, 586-594, 2005). Although imposing Thivet's realizability condition seems to result in overprediction of the far field pressure wave amplitudes, applying realizability and shock unsteadiness corrections overally yields a better agreement with the measurements.

1 INTRODUCTION

The fouling of heat transfer surfaces in kraft recovery boilers is a significant concern for the pulp and paper industry. The usual approach to controlling fouling is the use of so-called "sootblowers," that utilize boiler steam to generate supersonic steam jets that are literally used to knock deposits off of the boiler tubes. Sootblower nozzles are nominally designed to expand the steam to ambient pressure at the nozzle exit. In reality, sootblower jets never operate at exactly the design condition, and so the jet pressure at the nozzle exit is never precisely the ambient boiler pressure.

When the pressure of a supersonic jet at a nozzle exit is higher than the ambient pressure, shock and expansion waves (the so-called multi-cell shock structure) form, through which the pressure of the flow field drops to the ambient value. Underexpanded free jets involve a simple flow geometry, yet very complicated phenomena, because of these shock waves and their interaction with turbulent mixing. The flow structure of an underexpanded jet can be considered to consist of near and far field areas. The near field includes the first few shock cells from the nozzle exit, where the flow field is largely characterized by the inviscid shock structure, and where turbulence is not significant. Further downstream, turbulence influences the far field behavior, as turbulent mixing reaches the jet centerline and so engulfs the whole flow field.

Because of the complex nature of the flow structure, numerical simulation of underexpanded jets is challenging. Some have approached the problem by using separate schemes for the supersonic and subsonic areas of the flow field. This includes solving the inviscid equations for the shock cell region of the jet, setting the turbulence viscosity to zero for all mesh points in that area [1, 4, 5, 6]. Using this approach yielded satisfactory prediction of some available measurements. Other researchers have used compressibility-corrected $k - \varepsilon$ turbulence models to simulate mildly and highly underexpanded jets [2, 3, 8]; the models that considered dilatational compressibility effects (e.g. Sarkar et al. [17]) showed the best overall performance. How-

ever, as pointed out by Wilcox [27], the model of Sarkar et al. is based on early DNS results and is not universally accepted by all researchers. In fact, as will be discussed later, the effects of the dilatational compressibility are usually negligible compared to the structural compressibility [9, 27].

Here we focus on the simulation of an underexpanded supersonic air jet exhausting into still air, and compare the results to some available experimental data. The results were computed using CFDLib 3.02, a CFD code developed at the Los Alamos National Laboratory. The performance of a modified $k-\varepsilon$ turbulence model is evaluated and discussed. The corrections to the turbulence model account for structural compressibility, realizability condition, and shock unsteadiness.

2 METHODOLOGY

2.1 Governing Equations

To calculate the motion of a compressible flow, the Favre averaged equations of conservation of mass, momentum and energy must be solved,

$$\bar{\rho}\,\dot{\bar{v}} = \frac{\partial \tilde{u}_i}{\partial x_i} \tag{1}$$

$$\bar{\rho}\,\dot{\tilde{u}}_i = -\frac{\partial \bar{p}}{\partial x_i} + \frac{\partial \bar{t}_{ij}}{\partial x_j} + \frac{\partial \lambda_{ij}}{\partial x_j} \tag{2}$$

$$\bar{\rho}\dot{\tilde{E}} = -\frac{\partial \bar{p}\tilde{u}_j}{\partial x_j} + \frac{\partial \tilde{u}_i \bar{t}_{ij}}{\partial x_j} + \tilde{u}_i \frac{\partial \lambda_{ij}}{\partial x_j} - \frac{\partial q_{Lj} + q_{Tj}}{\partial x_j} + \bar{\rho}\varepsilon \tag{3}$$

along with an equation of state $\bar{p} = \bar{\rho} R \tilde{T}$. The left hand side of the conservation equations are written in Lagrangian terms.

2.2 Turbulence Model

The turbulence model is the standard $k-\varepsilon$ model, with modifications applied to account for the effects of structural compressibility, realizability, and shock unsteadiness. The turbulence kinetic energy k for a compressible flow is [27]

$$\bar{\rho}\dot{k} = \lambda_{ij}\frac{\partial \tilde{u}_i}{\partial x_j} - \bar{\rho}\varepsilon + \frac{\partial}{\partial x_j}[(\mu + \frac{\mu_T}{\sigma_k})\frac{\partial k}{\partial x_j}] \tag{4}$$

The Favre average Reynolds stress tensor, λ_{ij}, can be approximated using the Boussinesq approximation as

$$\lambda_{ij} = -\overline{\rho\, u_i'' u_j''} = 2\mu_T(S_{ij} - \frac{1}{3}S_{kk}\delta_{ij}) - \frac{2}{3}\bar{\rho}k\delta_{ij} \tag{5}$$

where $\tilde{S}_{ij}$ is the mean strain rate defined as

$$\tilde{S}_{ij} = \frac{1}{2}(\frac{\partial \tilde{u}_i}{\partial x_j} + \frac{\partial \tilde{u}_j}{\partial x_i}) \tag{6}$$

The so-called pressure dilatation, pressure diffusion, and pressure work terms are neglected in Equation 4. The pressure dilatation and pressure diffusion terms are very small for both mixing layers and boundary layers, based on DNS research [27], and as little is known about the pressure work term, it is usually neglected as well [27].

The equation for ε, the second auxiliary variable of the $k-\varepsilon$ model, is postulated as

$$\bar{\rho}\dot{\varepsilon} = C_{\varepsilon 1}\frac{\varepsilon}{k}\lambda_{ij}\frac{\partial \tilde{u}_i}{\partial x_j} - C_{\varepsilon 2}\bar{\rho}\frac{\varepsilon^2}{k} + \frac{\partial}{\partial x_j}[(\mu + \frac{\mu_T}{\sigma_\varepsilon})\frac{\partial \varepsilon}{\partial x_j}] \tag{7}$$

where $C_{\varepsilon 1}$, $C_{\varepsilon 2}$ and σ_ε are constant closure coefficients, and from the dynamic eddy viscosity $\mu_T = C_\mu \bar{\rho}\frac{k^2}{\varepsilon}$, C_μ is an additional coefficient. These closure coefficients are obtained by calibration of the model versus experimental data. For the standard $k-\varepsilon$ model, the values of the coefficients are $C_{\varepsilon 1}$=1.44, $C_{\varepsilon 2}$=1.92, σ_k=1.0, σ_ε=1.3 and C_μ=0.09.

The next three sections present modifications to the standard model, that were implemented in CFDLib. The first is that of Tandra [23], while the other two were implemented as part of the present work.

2.2.1 Compressibility Effects

Compressibility effects may be categorized into two groups: those related to the change in the structure of the turbulence kinetic energy distribution, and those related to the extra dilatational terms that appear in the compressible turbulence kinetic energy equation. DNS research has shown that the effects of the dilatational compressibility are usually negligible compared to the structural effects [9, 27].

DNS results [16] show that in a compressible turbulent shear layer the spatial distribution of k varies tremendously, and so the stream-wise component of k increases with the compressibility level [9]. Using the DNS results of Sarkar [16] for compressible turbulent shear flow, Heinz [9] suggested that

$$C_\mu = 0.07\exp(-0.4M_g) \tag{8}$$

where M_g, the gradient Mach number, characterizes the strength of compressibility. Sarkar [16] suggested

$$M_g = \frac{S_g l_g}{a} \tag{9}$$

where $S_g = \frac{\partial U_1}{\partial x_2}$ is the mean shear rate, U_1 and x_2 are the stream-wise mean velocity and the shear direction coordinate, respectively, l_g is the correlation length of the stream-wise fluctuating velocities in the shear direction, and a is the local sound speed. The greater the gradient Mach number, the stronger the compressibility effects.

Tandra et al. [24] suggested that for a general flow the mean shear rate be calculated as

$$S_g = \sqrt{2[\tilde{S}_{ij}\tilde{S}_{ji} - \frac{1}{3}S_{kk}^2]} \tag{10}$$

where $\tilde{S}_{ij}$ is the local mean shear rate, and that the value of l_g be calculated in a way similar to the characteristic length scale used in Prandtl's one-equation turbulence model [27]

$$l_g = C_D \frac{k^{3/2}}{\varepsilon} \tag{11}$$

where C_D is a closure coefficient usually considered to be 0.09.

The $k - \varepsilon$ model along with the above mentioned structural compressibility correction has been validated against a wide range of available data corresponding to properly expanded (and therefore shock wave free) high speed jet flows; the simulations satisfactorily predicted all of the examined cases. But as will be discussed in detail later in this paper, the model fails to satisfactorily predict the behavior of underexpanded jets. It seems that the structural compressibility correction is not sufficient to properly model the shock wave/turbulence interaction, which is not surprising. It is well known that two-equation turbulence models predict a spuriously large growth of the turbulent kinetic energy, and thus eddy viscosity, near stagnation points [7], shock waves [21], massive separations, and generally anywhere in the flow field that experiences large strain rates [20]. Underexpanded jets are largely characterized by the shock/turbulence interaction, and so corrections should be applied to take this phenomenon into account. Here, two approaches are examined to suppress the erroneous growth of the eddy viscosity in the highly shock wave-dominated flow field of underexpanded jets: imposition of a realizability condition, and consideration of shock unsteadiness effects. These are addressed in the next two sections.

2.2.2 Realizability Condition

Durbin [7] suggested suppressing the eddy viscosity by imposing the realizability constraint. Since $k = \frac{1}{2}\overline{u_k'' u_k''}$, we should have (for each $i = 1, 2, 3$)

$$\overline{u_i''^2} \geq 0 \tag{12}$$

$$\overline{u_i''^2} \leq 2k \tag{13}$$

The first condition is more restrictive than the second; in fact, the second constraint follows if the first is met (for proof see [7]). Using the Boussinesq approximation ($\overline{u_i''^2} \simeq -2\nu_T S_{ii} + \frac{2}{3}k$) and Equation 12, we have

$$\nu_T \leq \frac{k}{3S_{ii}} \tag{14}$$

which implies that

$$\nu_T \leq \frac{k}{3\max(S_{ii})} \tag{15}$$

Durbin further reduced the form of this condition by assuming that flow is incompressible

$$\nu_T \leq \frac{1}{\sqrt{6}}\frac{k}{S_{Durbin}} \tag{16}$$

where $S_{Durbin}(= \sqrt{S_{ij}S_{ji}})$ is a measure of the mean strain rate of the flow. Tandra [2005] suggested that when this correlation is used for compressible flows, as it is here, S_{Durbin} be re-defined as

$$S_{Durbin} = \sqrt{S_{ij}S_{ji} - \frac{1}{3}S_{kk}^2} \tag{17}$$

From here on, we refer to Equation 15 as the compressible realizability condition, and Equation 16 as Durbin's realizability condition. To meet realizability, the eddy viscosity should then be calculated as

$$\nu_T = \min(C_\mu \frac{k^2}{\varepsilon}, C_{Durbin}\nu_{T,max}) \tag{18}$$

where $\nu_{T,max}$ is the maximum possible eddy viscosity that meets the realizability constraint and can be calculated from either Equation 15 or 16. C_{Durbin} is an empirical constant less than 1, that is used to obtain agreement with experimental data [7]. Thivet et al. [25] suggested setting C_{Durbin} to 0.5.

Thivet et al. [26] also proposed a condition on eddy viscosity for imposing the realizability condition

$$\nu_T = \min(C_\mu \frac{k^2}{\varepsilon}, \sqrt{C_\mu}\frac{k}{S_{Thivet}}) \tag{19}$$

where S_{Thivet} is defined as

$$S_{Thivet} = \sqrt{2}S_{Durbin} \tag{20}$$

We refer to this as Thivet's realizability condition. Comparing DNS results of isotropic turbulence through a normal shock wave with the results obtained from a $k-\varepsilon$ model, Sinha et al. [21] concluded that the Durbin and Thivet correlations improve the prediction of the turbulence kinetic energy to some extent, and yield the correct trend by reducing eddy viscosity in the vicinity of shocks.

2.2.3 Effects of Shock Unsteadiness

It has been shown that shock unsteadiness plays an important role in the interaction of turbulence with shock waves [21]. Shock unsteadiness causes the mean shock thickness to increase, and seems to be correlated with turbulence fluctuations [11] that distort the shock wave front and lead to unsteady displacements [13, 28]. Specifically in underexpanded jets, shock unsteadiness has been observed experimentally [14, 15]. Sinha et al. [21] suggested that over-prediction of turbulence production in the presence of shock waves is due to the fact that shock unsteadiness is not taken into account in turbulence models.

Sinha et al. proposed a modification to the $k-\varepsilon$ model, based on the effect of a normal shock wave on an isotropic homogeneous uniform turbulent flow. In order to account for the unsteady motion of a shock, Sinha et al. wrote the transport equations in the frame of reference of the shock. Assuming that the distortion of the shock from its mean position is $x = \zeta(y, z, t)$ (where x is the direction normal to the shock, y and z are the other two directions, and t is time), a new term $\widetilde{u''\zeta_t}$ appears in the turbulence kinetic energy equation. Sinha et al. modeled the new term as

$$\widetilde{u''\zeta_t} = b_1 \widetilde{u''^2} \tag{21}$$

where b_1 is a coefficient calculated as a function of the local Mach number M,

$$b_1 = 0.4(1 - e^{1-M}) \tag{22}$$

which is a fit of linear analysis results [12, 10, 11] for $\widetilde{u''\zeta_t}/\widetilde{u''^2}$. Based on this, Sinha et al. proposed that the production term $\lambda_{ij}\frac{\partial \tilde{u}_i}{\partial x_j}$ in the k-equation be replaced by $-\frac{2}{3}\bar{\rho}kS_{ii}(1 - b_1)$.

Sinha et al. further proposed a correction to the ε-equation by changing the value of $C_{\varepsilon 1}$, again based on the results of linear analysis,

$$C_{\varepsilon 1} = 1.25 + 0.2(M - 1) \tag{23}$$

Note that these changes should be applied only in supersonic regions of a flow field. Hereafter, this shock unsteadiness correction will be referred to as the Sinha [2003] model.

The Sinha [2003] model is derived based on the interaction of homogeneous and isotropic turbulence with a normal shock wave in a one dimensional flow. More recently, Sinha et al. [22] proposed another correction to generalize their model to flows with additional mean gradients. From Equation 4, the turbulence production term is $P_k = \lambda_{ij}\frac{\partial \tilde{u}_i}{\partial x_j}$. Using Equation 5, this can be written as

$$P_k = \mu_T(2S_{ij}S_{ji} - \frac{2}{3}S_{kk}^2) - \frac{2}{3}\bar{\rho}kS_{kk} \tag{24}$$

Sinha et al. [22] suggested replacing μ_T in Equation 24 with $c_\mu^{'}\mu_T$, where

$$c_\mu^{'} = 1 - f_s[1 + \frac{1}{\sqrt{3}}\frac{b_1^{'}\varepsilon}{kS_{Thivet}C_\mu}] \tag{25}$$

and

$$f_s = \frac{1}{2} - \frac{1}{2}\tanh(5\frac{S_{kk}}{S_{Thivet}} + 3) \tag{26}$$

and S_{Thivet} is defined by Equation 20. Equation 26 defines f_s such that f_s is close to 1 in highly compressed regions and close to 0 otherwise. We refer to this correction as Sinha [2005] model. The performance of both Sinha models is evaluated in this paper.

2.3 Numerical Scheme

The CFDLib code is based on a cell-centered finite-volume method. The scheme is explicit and utilizes a time split operator for advancing the averaged flow variables in time, consisting of so-called Lagrangian and Eulerian time advancement phases. To calculate the fluxes on the cell boundaries, a space centered, locally time advanced method is used. Flux limiters are used to stabilize the numerical solution. The flux can then be viewed as a combination of a low order and a high order flux, which is common to most TVD (total variable diminishing) schemes.

3 RESULTS AND DISCUSSION

The measurements of Seiner and Norum [19] of an underexpanded air jet are used to asses the various corrections to the turbulence model. This data set is frequently cited and used to asses numerical models. Simulations were run in a 2-D axisymmetric coordinate system. The pressure ratio (ratio of the exit to ambient pressure) at the jet exit was 1.45 and the exit Mach number was 2.0. Based on this values, the inlet boundary conditions (velocity, density and temperature) corresponding to the jet exit were calculated. Ambient pressure was applied as a boundary condition far from the jet centerline. Based on

the nozzle exit diameter D_{exit}, the size of the computational domain was $20D_{exit}$ in the axial and $5D_{exit}$ in the radial directions. The calculations were also performed on larger domains to confirm that the results did not depend on domain size. The simulations were also run on different meshes.

Figure 1 shows calculated centerline normalized pressure versus the axial distance normalized by the nozzle exit radius r_{exit} ($=D_{exit}/2$) on different computational meshes and compared to the experimental data, using the compressibility-corrected $k-\varepsilon$ model (not including the realizability and shock unsteadiness corrections). The uniform mesh size, Δ, varies from $\Delta = D_{exit}/10$ to $\Delta = D_{exit}/40$. As can be seen, the simulations predict the position of the first few shock cells correctly, but the solution is too diffusive as the amplitude of even the first shock waves is underpredicted, especially on a coarse mesh. Further downstream, the diffusion is so high that the shock and expansion waves are damped, even on the finest mesh. At mesh size of $D_{exit}/20$-$D_{exit}/40$ the solution seems to become independent of the computational mesh. This agrees with Fairweather and Ranson [8] who indicated that the solution for an underexpanded jet is mesh independent at a mesh size of $D_{exit}/32$.

The high level of dissipation in the simulations is related to the turbulence model, and so we now consider the inclusion of the realizability condition and shock unsteadiness. All of the tests were carried out on either or both $\Delta = D_{exit}/20$ and $\Delta = D_{exit}/40$ meshes. To begin, we ran an inviscid simulation with no turbulence model (Figure 2). As expected, the results are not in good agreement with the data, but the overdamping of the pressure wave in the far field is eliminated. This confirms that turbulence is responsible for the high level of diffusivity in the previous numerical solutions.

Figure 3 shows the results when Durbin's realizability model is imposed. Following Thivet et al. [25] C_{Durbin} was set to 0.5. As can be seen, imposing the realizability condition improves the simulation results in the far field, as the overprediction of the eddy viscosity is at least partially eliminated. However, the location of some shock cells far downstream is not properly predicted. Also as expected, the results computed on the finer mesh ($\Delta = D_{exit}/40$) are less diffusive than those computed at $\Delta = D_{exit}/20$.

Figure 4 presents results when the realizability constraint of Thivet et al. is applied. At least for this case, the Thivet's constraint seems to lead to better agreement with the measurements than Durbin's constraint, as the location of the far field shock cells is more accurately predicted. On the other hand, the amplitudes of the far field shock cells seem to be overestimated. The amplitude of the pressure waves are expected to decrease as one gets further downstream from the jet exit, due to the dissipation that results from the turbulent mixing of the flow field. This is not properly captured when Thivet's realizability condition is enforced, as is especially apparent in the finer mesh results. Other than this, the agreement with the measurements is fairly reasonable.

Figure 5 shows the results when Sinha [2003] is applied, and shows that these modifications do not make a significant difference to the results. This is not surprising; Sinha et al. suggested these corrections based on the interaction of homogeneous isotropic turbulence with a normal shock wave in a uniform 1-D flow. The case of an underexpanded jet involves much more complex phenomena than this. Sinha [2005] correction yields better agreement with the present data, by eliminating the over-damping of the pressure waves in the far field, as shown in Figure 6.

Finally, Figure 7 shows the results of applying Sinha [2005] correction and Thivet's realizability condition together. The result is similar to that of Figure 4, obtained by applying Thivet's constraint alone. Again, the far field pressure wave amplitudes are somewhat overpredicted.

4 CONCLUSION

We examined the simulation of underexpanded jets accounting for the turbulence/shock wave interaction. To achieve this, realizability conditions and shock unsteadiness corrections were applied to a compressibility-corrected $k-\varepsilon$ turbulence model. Although imposing Thivet's realizability condition (alone or together with the shock unsteadiness correction) seems to result in overprediction of the far field pressure wave amplitudes, applying these corrections yield better agreement with the measurements.

References

[1] S.G. Chuech, M. Lai, and G.M. Faeth. Structure of turbulent sonic underexpanded free jets. *AIAA Journal*, 27(5):549-559, 1989

[2] P.S. Cumber, M. Fairweather, and S.A.E.G. Falle. Predictions of the structure of turbulent, moderately underexpanded jets. *Journal of Fluids Engineering, Transactions of the ASME*, 116(4):707-713, 1994

[3] P.S. Cumber, M. Fairweather, and S.A.E.G. Falle. Predictions of the structure of turbulent, highly underexpanded jets. *Journal of Fluids Engineering, Transactions of the ASME*, 117(4):599-604, 1995

[4] S. Dash and D. Wolf. Interactive phenomena in supersonic jet mixing problems, Part I:

Phenomenology and numerical modeling techniques. *AIAA Journal*, 22(7):905-913, 1984

[5] S.M. Dash and D.E. Wolf. Interactive phenomena in supersonic jet mixing problems, Part II: Numerical studies. *AIAA Journal*, 22(10):1395-1404, 1984

[6] S.M. Dash, D.E. Wolf, and J.M. Seiner. Analysis of turbulent underexpanded jets, Part I: Parabolized Navier-Stokes model, SCIPVIS. *AIAA Journal*, 23(4):505-514, 1985

[7] P.A. Durbin. On the k-3 stagnation point anomaly. *International Journal of Heat and Fluid Flow* 17(1):89-90, 1996

[8] M. Fairweather and K.R. Ranson. Prediction of underexpanded jets using compressibility-corrected, two-equation turbulence models. *Progress in Computational Fluid Dynamics*, 6(1-3):122-128, 2006

[9] S. Heinz. A model for the reduction of the turbulent energy redistribution by compressibility. *Physics of Fluids*, 15(11):3580-3583, 2003

[10] S. Lee, S.K. Lele, and P. Moin. Interaction of isotropic turbulence with shock waves: Effect of shock strength. *Journal of Fluid Mechanics*, 340:225-247, 1997

[11] K. Mahesh, S.K. Lele, and P. Moin. The influence of entropy fluctuations on the interaction of turbulence with a shock wave. *Journal of Fluid Mechanics*, 334:353-379, 1997

[12] K. Mahesh, S. Lee, and S.K. Lele. Interaction of an isotropic field of acoustic waves with a shock wave. *Journal of Fluid Mechanics*, 300:383-407, 1995

[13] F.K. Moore. Unsteady oblique interaction of a shock wave with a plane disturbance. *NACA TN 2879*, 1954

[14] J. Panda. Shock oscillation in underexpanded screeching jets. *Journal of Fluid Mechanics*, 363:173-198, 1998

[15] J. Panda and R.G. Seasholtz. Measurement of shock structure and shock-vortex interaction in underexpanded jets using Rayleigh scattering. *Physics of Fluids*, 11(12):3761-3777, 1999

[16] S. Sarkar. The stabilizing effect of compressibility in turbulent shear flow. *Journal of Fluid Mechanics*, 282:163-186, 1995

[17] S. Sarkar, G. Erlebacher, and M.Y. Hussaini. Analysis and modeling of dilatational terms in compressible turbulence. *Journal of Fluid Mechanics*, 227:473-493, 1991

[18] J.M. Seiner, S.M. Dash, and D.E. Wolf. Analysis of turbulent underexpanded jets. Part II: Shock noise features using SCIPVIS. *AIAA Journal*, 23(5):669-677, 1985

[19] J.M. Seiner and T.D. Norum, Aerodynamic aspects of shock containing jet plumes. *AIAA Paper 80-0965*, 1980

[20] T. Shih, W.W. Liou, and A. Shabbir. New $k-\varepsilon$ eddy viscosity model for high Reynolds number turbulent flows. *Computers and Fluids*, 24(3):227-238, 1995

[21] K. Sinha, K. Mahesh, and G.V. Candler. Modeling shock unsteadiness in shock/turbulence interaction. *Physics of Fluids*, 15(8):2290-2297, 2003

[22] K. Sinha, K. Mahesh, and G.V. Candler. Modeling the effect of shock unsteadiness in shock/turbulent boundary-layer interactions. *AIAA Journal*, 43(3):586-594, 2005

[23] D. Tandra. Development and application of a turbulence model for a sootblower jet propagating between recovery boiler superheater platens. *PhD Thesis, University of Toronto*, 2005

[24] D.S. Tandra, A. Kaliazine, and D.E. Cormack. Numerical simulation of supersonic jet flow using a modified $k-\varepsilon$ model. *International Journal of Computational Fluid Dynamics*, 20(1):19-27, 2006

[25] F. Thivet, D.D. Knight, and A.A. Zheltovodov. Importance of limiting the turbulent stresses to predict 3D shock wave/boundary layer interactions. *23rd Symposium on Shock Waves*, Paper No. 2761, 2001

[26] F. Thivet, D.D. Knight, and A.A. Zheltovodov. Insights in turbulence modeling for crossing-shock-wave/boundary-layer interactions. *AIAA Journal*, 39(6):985-995, 2001

[27] D.C. Wilcox. Turbulence Modeling for CFD. *DCW Industries*, 2004

[28] G.P. Zank, Y. Zhou, and W.H. Matthaeus. The interaction of turbulence with shock waves: A basic model. *Physics of Fluids*, 14(11):3766-3774, 2002

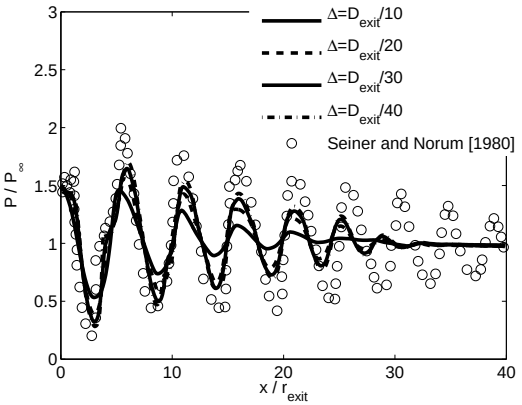

Figure 1: Normalized pressure along the centerline of an underexpanded jet; results from different computational meshes.

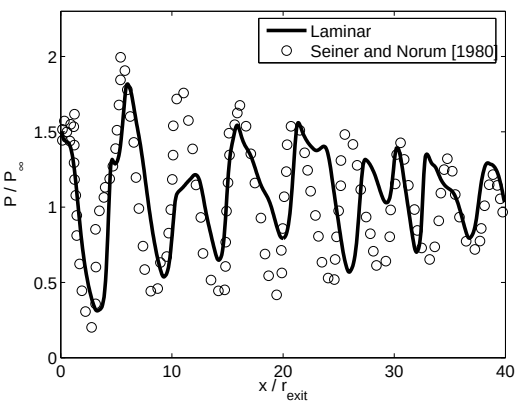

Figure 2: Inviscid (laminar) calculation of the flow field, $\Delta = D_{exit}/20$.

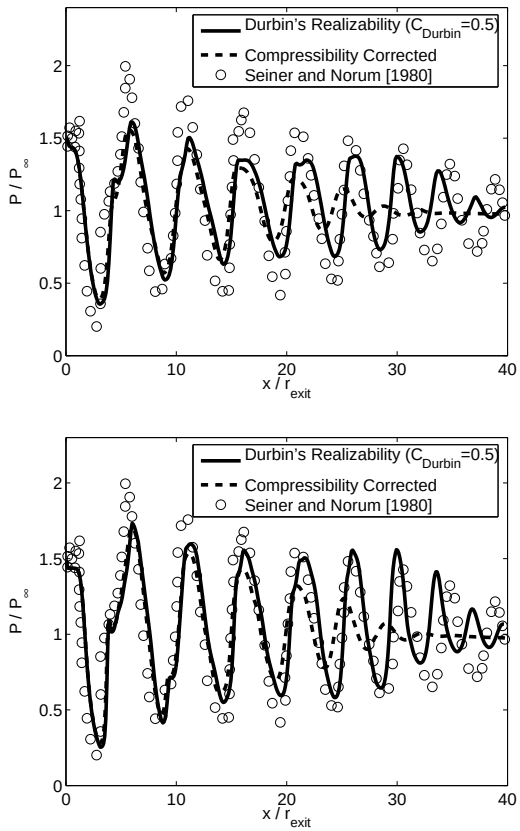

Figure 3: Calculations with Durbin's realizability condition: $\Delta = D_{exit}/20$ (top), and $\Delta = D_{exit}/40$ (bottom); C_{Durbin}=0.5.

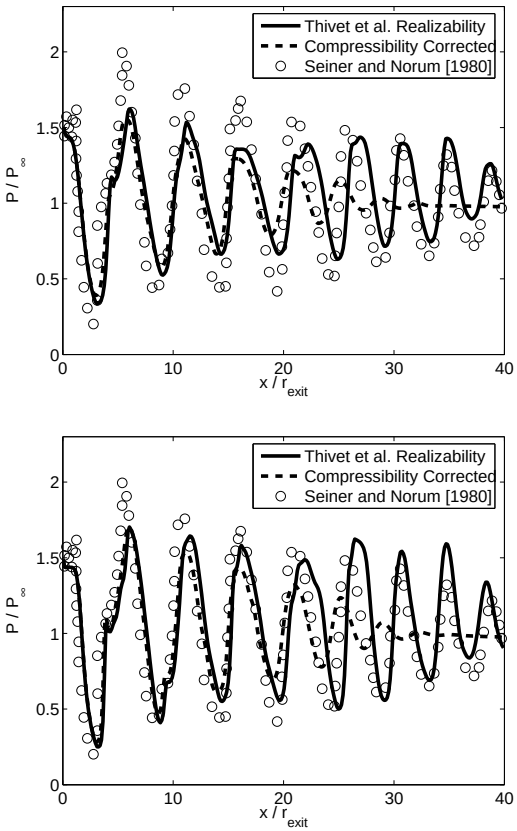

Figure 4: Calculations with Thivet's realizability condition: $\Delta = D_{exit}/20$ (top), and $\Delta = D_{exit}/40$ (bottom).

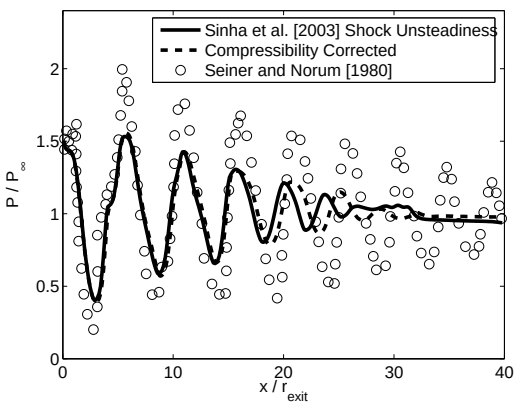

Figure 5: Calculation with Sinha [2003] model (a shock unsteadiness correction), $\Delta = D_{exit}/20$.

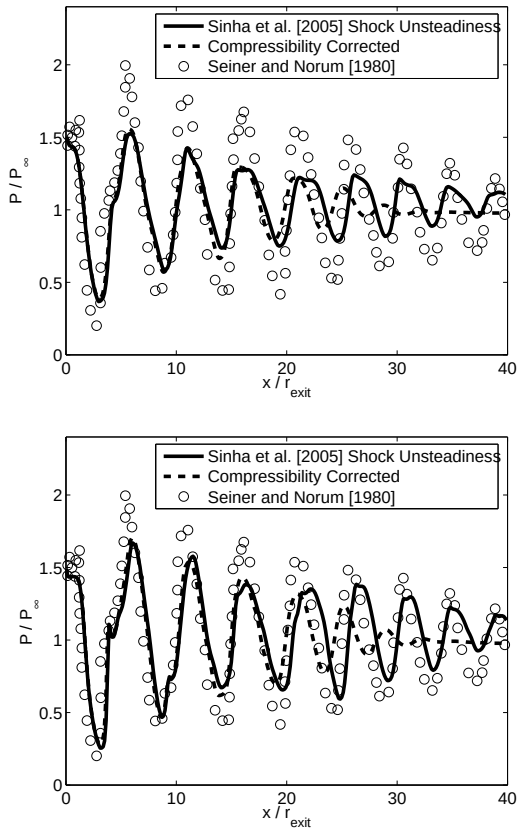

Figure 6: Calculations with Sinha [2005] model (a shock unsteadiness correction): $\Delta = D_{exit}/20$ (top), and $\Delta = D_{exit}/40$ (bottom).

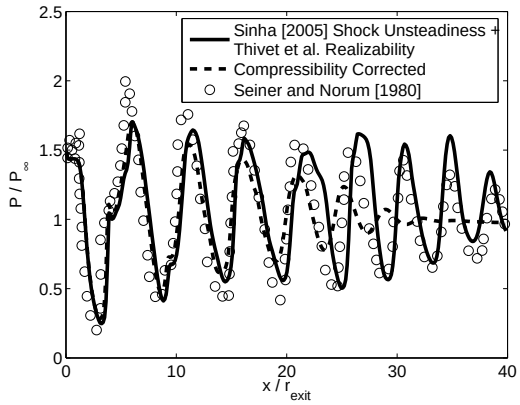

Figure 7: Calculations with both Sinha [2005] and Thivet's realizability corrections, $\Delta = D_{exit}/40$.